Int. J. Solids Structures Vol. 27, No. 12, pp. 1537–1550, 1991
Printed in Great Britain.

0020-7683/91 $3.00 + .00

THE INFLUENCE OF INCLUSION SHAPE ON THE OVERALL ELASTOPLASTIC BEHAVIOR OF A TWO-PHASE ISOTROPIC COMPOSITE

Y. P. QIU and G. J. WENG
Department of Mechanics and Materials Science, Rutgers University,
New Brunswick, NJ 08903, U.S.A.

(*Received* 13 *October* 1989; *in revised form* 4 *June* 1990)

Abstract—A mean-field, approximate theory is developed for the determination of the overall stress–strain relation of a two-phase composite, consisting of randomly oriented elastic, spheroidal inclusions and a ductile matrix. The theory is intended for a low-volume concentration of inclusions. It is versatile enough to provide results under any proportionally increasing combined stresses, and yet simple enough to require no iterations. To preserve the virtue of simplicity, the simpler deformation theory is used over the incremental one. More so than the elastic behavior, the elastoplastic response of the composite is found to be extremely sensitive to the inclusion shape, with the discs providing the most remarkable reinforcement. Explicit results of the overall secant moduli are established for the three extreme inclusion shapes of disc, needle (fiber) and sphere. An interesting consequence of this analysis is that while both the particle and fiber-reinforced composites become plastically compressible, the disc-reinforced composite – as the ductile matrix itself – remains plastically incompressible. When applied to a silicon-carbide/aluminum system, the theory indicates that within the aspect ratio $\alpha < 10$, the prolate and oblate inclusions with inversed aspect ratios (i.e. α and $1/\alpha$) have almost the same effect on the flow stress of the composite, but beyond this the disc-oriented inclusions begin to show a more superior influence. The theory also compares reasonably with the experimental data when the carbides exist in the form of randomly oriented platelets, with $\alpha = 1/4$.

1. INTRODUCTION

This paper is concerned with the determination of the overall stress–strain relation of a two-phase isotropic composite, in which elastic, spheroidal inclusions of a given aspect ratio are randomly distributed in a ductile matrix. The inclusions and the matrix are assumed to be perfectly bonded together, without any void nucleation or growth. Both phases are taken to be elastically isotropic, and the matrix may possess a distinct yield point and nonlinear work-hardening characteristics. This class of composite covers a wide range of inclusions; they may range from thin discs to oblate shape, from spheres to prolate or short fibers, and all the way to needles or continuous fibers. Our objective here is to develop a simple, albeit approximate, theory which is capable of accounting for the effect of inclusion shape on the overall elastoplastic behavior of the composite at a low concentration of inclusions. Special attention will be given to the three extreme shapes: disc, fiber and sphere.

The method to be presented is based upon the theoretical framework recently developed by Tandon and Weng (1988) for particle-reinforced plasticity. It evolved from the second writer's study on polycrystal plasticity and composite elasticity (Weng, 1982, 1984), and is intended for proportionally increasing (not nonradial or cyclic) combined stress. In this theory the auxiliary interaction problem between a single inclusion and a plastically deforming matrix is treated with Hill's (1965) weakening constraint power of the matrix, whereas the inclusion–inclusion interaction at a finite volume concentration is considered by Mori and Tanaka's (1973) mean-field approach. The theoretical foundation leading to such a development was given extensively in that earlier paper where, among others, it has also been demonstrated that, up to 47% of particle concentration, the theoretical prediction was in reasonable agreement with the experimental data of a silica particle/epoxy matrix composite.

The elastic counterpart of the present problem has been studied by Tandon and Weng (1986), whose formulations will prove to be useful here. Also using Mori–Tanaka's mean-field theory, they found that, when the aspect ratio of the randomly oriented inclusions varies from that of a disc to a needle, the calculated bulk and shear moduli of the composite always lie between the Hashin and Shtrikman (1963) bounds. As also disclosed earlier by Weng (1984), the results with spherical inclusions coincide with their lower bounds if the matrix is the softer phase, and conversely they coincide with the upper bounds. Consistent with Wu's (1966) investigation, the disc type of reinforcement was found to be superior to the needle type. The predicted elastic moduli have also been shown to be in good accord with the test data for some particle-reinforced and void-containing materials (see Weng, 1984).

As in Tandon and Weng (1988), the method to be presented is a mean-field one. While it is appreciated that, in the estimate of a nonlinear effective property, a local approach which can account for the point-to-point variation of the stress field is usually more accurate than the mean-field approach, such an approach normally can only be employed to particle—or unidirectionally-aligned fiber—composites (see for instance Chu and Hashin, 1971; Hill, 1964; Accorsi and Nemat-Nasser, 1986; Teply and Dvorak, 1988). Indeed, even with such simple microgeometries the number of studies, due to the difficulty involved in the material nonlinearity, has been rather limited. For a randomly-oriented composite under a combined stress, such a local approach does not seem to be possible at present, and the mean-field approach—which has already proven to be able to capture the essence of a particle-reinforced plasticity—is believed to be a reasonable approximation. It should be recognized, however, that since local yielding is not accounted for, the yield stress of the composite predicted by this theory is always higher than that predicted by the local analysis. Initial local yielding in retrospect involves only a very small volume fraction of the matrix, and therefore its manifestation on the overall stress–strain curve of the composite will not be significant. But the approximation inherent in the mean-field approach for a physically nonlinear problem will necessitate the application to be limited to the low-volume concentration range, under which the majority of the deformation field in the ductile matrix is more uniform.

2. CONSTITUTIVE EQUATIONS OF THE CONSTITUENTS

In the two-phase system the randomly oriented spheroidal inclusions will be referred to as phase 1, and the ductile matrix as phase 0. The isotropic bulk and shear moduli of the rth phase will be denoted by κ_r and μ_r, respectively, and its volume fraction by c_r.

Since the theory is intended only for monotonic, proportional loading, the deformation theory—instead of the incremental theory—will be used to describe the multiaxial stress–strain relation of the ductile matrix. Under a uniaxial tension the flow stress–plastic strain relation of most metals can usually be represented by the modified Ludwik equation

$$\sigma = \sigma_y + h \cdot (\varepsilon^p)^n, \tag{1}$$

where σ is the flow stress at the plastic strain ε^p, and σ_y, h and n are the initial yield stress, strength coefficient, and work-hardening exponent, in turn. These three material constants can be readily determined from a tensile stress–strain curve.

The "secant" Young's modulus of the matrix, defined by the ratio of tensile stress to the tensile strain—which is the sum of the elastic and plastic components—is given by

$$E_0^s = \frac{1}{\dfrac{1}{E_0} + \dfrac{\varepsilon^p}{\sigma_y + h \cdot (\varepsilon^p)^n}}, \tag{2}$$

where E_0 is its ordinary Young's modulus. With respect to the undeformed state, the "secant" bulk and shear moduli of the matrix are taken to satisfy the isotropic relation

$$\kappa_0^s = \frac{E_0^s}{3(1-2\nu_0^s)} = \kappa_0, \quad \mu_0^s = \frac{E_0^s}{2(1+\nu_0^s)}, \tag{3}$$

in terms of the "secant" Poisson ratio ν_0^s. The assumption of plastic incompressibility—which also results in $\kappa_0^s = \kappa_0$—further provides

$$\nu_0^s = \tfrac{1}{2} - (\tfrac{1}{2} - \nu_0)\frac{E_0^s}{E_0}, \tag{4}$$

in terms of Poisson's ratio ν_0. The plastic state of the matrix is therefore fully characterized by any of E_0^s, μ_0^s or ν_0^s.

Since the ductile matrix is usually in a triaxial stress state, it is useful to generalize (1) to

$$\sigma^* = \sigma_y + h\cdot(\varepsilon^{p^*})^n, \tag{5}$$

in terms of von Mises' effective stress and strain, defined respectively by

$$\sigma^* = (\tfrac{3}{2}\sigma'_{ij}\sigma'_{ij})^{1/2}, \quad \varepsilon^{p^*} = (\tfrac{2}{3}\varepsilon^p_{ij}\varepsilon^p_{ij})^{1/2}, \tag{6}$$

where σ'_{ij} is the deviatoric stress tensor. Then in a triaxial stress state the secant Young's modulus becomes

$$E_0^s = \frac{1}{\dfrac{1}{E_0} + \dfrac{\varepsilon^{p^*}}{\sigma_y + h\cdot(\varepsilon^{p^*})^n}}. \tag{7}$$

3. THE EFFECTIVE SECANT MODULI OF A RANDOMLY ORIENTED COMPOSITE

A detailed derivation which started from Hill's (1965) inclusion-matrix interaction—by way of Berveiller and Zaoui's (1979) modification under proportional loading to incorporate Mori and Tanaka's (1973) method, can be found from Tandon and Weng (1988) for particle-reinforced plasticity. We now extend such a formulation to the condition where inclusions are randomly oriented in the matrix. Familiar symbolic notation—where a second-order tensor is denoted by a bold-faced Greek letter and a fourth-order tensor by an ordinary capital letter—will for brevity be employed in the first half of this section.

The microgeometry of a two-phase, isotropic composite with randomly oriented spheroidal inclusions is schematically shown in Fig. 1, in which the material axes are denoted

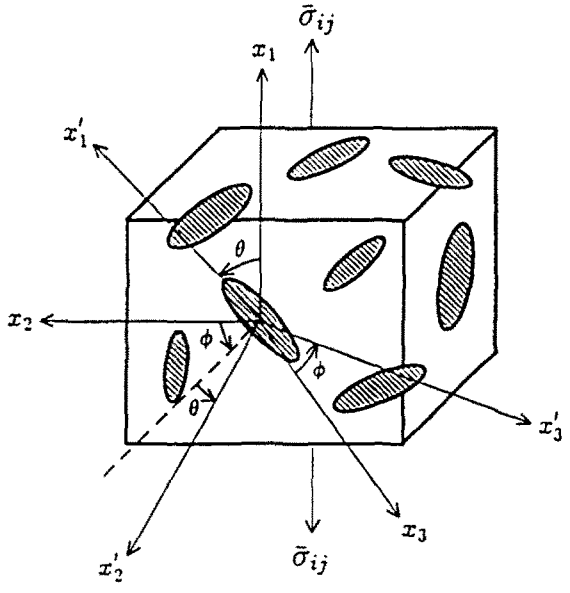

Fig. 1. The isotropic composite model with randomly oriented elastic, spheroidal inclusions and ductile matrix.

by x_i, and the local, oriented axes by x_i', with x_1' aligned along the symmetric line of the considered inclusion. Now let the composite be subjected to an external traction given rise to a uniform stress $\bar{\sigma}$, and denote the (yet unknown) secant moduli tensor of its matrix phase by L_0^s. To facilitate the analysis we also introduce at this instant a linearly elastic comparison material also with a moduli tensor L_0^s, and subject it to the same boundary traction. Such use of a linearly elastic comparison material in the prediction of a nonlinear effective property of the composite has also been suggested recently by Talbot and Willis (1987). The uniform strain in the comparison material is then given by

$$\varepsilon^0 = L_0^{s\,-1}\bar{\sigma}, \tag{8}$$

where $L_0^{s\,-1}$ is the inverse of L_0^s. This choice of comparison material differs somewhat from that suggested by Tandon and Weng (1988), where the nonlinear matrix was chosen for such a purpose. It is believed that this new choice will represent the current state of the matrix inside the composite system more accurately. Both choices, however, lead to the same overall response for the composite in the end.

The average stress and total strain of the matrix in the composite system usually differ from those of the comparison material, say by $\tilde{\sigma}$ and $\tilde{\varepsilon}$, respectively, so that the mean stress is given by

$$\sigma^{(0)} = \bar{\sigma} + \tilde{\sigma} = L_0^s(\varepsilon^0 + \tilde{\varepsilon}). \tag{9}$$

Similarly, the mean stress and strain of the inclusions, depending on their orientations, further differ from those of the surrounding matrix by some perturbed values, say, $\sigma^{pt}(\theta, \phi)$ and $\varepsilon^{pt}(\theta, \phi)$, respectively. Thus

$$\begin{aligned}\sigma^{(1)}(\theta, \phi) &= \bar{\sigma} + \tilde{\sigma} + \sigma^{pt}(\theta, \phi) = L_1[\varepsilon^0 + \tilde{\varepsilon} + \varepsilon^{pt}(\theta, \phi)] \\ &= L_0^s[\varepsilon^0 + \tilde{\varepsilon} + \varepsilon^{pt}(\theta, \phi) - \varepsilon^*(\theta, \phi)],\end{aligned} \tag{10}$$

where L_1 is the elastic moduli tensor of the inclusions and, being isotropic, is orientation-independent. The last equality represents Eshelby's (1957) equivalent-inclusion principle by which the equivalent transformation strain $\varepsilon^*(\theta, \phi)$ (or eigenstrain; Mura, 1987) is introduced into the regions of the comparison material, whose corresponding positions in the composite are occupied by the inclusions, to yield the same $\sigma^{(1)}$. As pointed out by Tandon and Weng (1988), the coefficient in the equivalent equation — in this case L_0^s in (10) — also represents the constraining power of the matrix; it thus weakens continuously, as first recognized by Hill (1965). The connection between $\varepsilon^{pt}(\theta, \phi)$ and $\varepsilon^*(\theta, \phi)$ is calculated in the linearly elastic comparison material with L_0^s, and, using Eshelby's S-tensor but now referred to the local principal axes x_i', is given by

$$\varepsilon_{local}^{pt}(\theta, \phi) = S_0^s \varepsilon_{local}^*(\theta, \phi), \tag{11}$$

where the transformation tensor S_0^s—corresponding to L_0^s—depends on the aspect ratio α (the ratio of the length to the diameter) of the inclusions and the secant Poisson ratio of the matrix ν_0^s. Its components for a general spheroid and for the three limiting shapes: (i) disc, (ii) fiber and (iii) sphere, are given in Appendix A.

The local, oriented strain components ε_{local} are related to the unoriented ones ε, or vice versa, through the usual transformation:

$$\varepsilon_{local} = Q\varepsilon Q^T, \quad \text{and} \quad \varepsilon = Q^T\varepsilon_{local}Q, \tag{12}$$

where the rotational matrix Q (not a fourth-order tensor) has the components

$$Q_{ij} = \begin{pmatrix} \cos\theta & \sin\theta\cos\phi & \sin\theta\sin\phi \\ -\sin\theta & \cos\theta\cos\phi & \cos\theta\sin\phi \\ 0 & -\sin\phi & \cos\phi \end{pmatrix}. \tag{13}$$

and the superscript T represents its transpose.

Now comparing (9) with (10), we find

$$\boldsymbol{\sigma}^{pt}(\theta,\phi) = L_0^s[\boldsymbol{\varepsilon}^{pt}(\theta,\phi) - \boldsymbol{\varepsilon}^*(\theta,\phi)]. \tag{14}$$

Furthermore, since $\bar{\boldsymbol{\sigma}} = \Sigma c_r \boldsymbol{\sigma}^{(r)}$, one has

$$\bar{\boldsymbol{\sigma}} = -c_1\langle\boldsymbol{\sigma}^{pt}(\theta,\phi)\rangle, \tag{15}$$

which in view of (14), also leads to

$$\bar{\boldsymbol{\varepsilon}} = -c_1\langle\boldsymbol{\varepsilon}^{pt}(\theta,\phi) - \boldsymbol{\varepsilon}^*(\theta,\phi)\rangle, \tag{16}$$

where the brackets $\langle\cdot\rangle$ represent the orientational average of the said quantity.

On the other hand, the total strain of the composite is given by $\bar{\boldsymbol{\varepsilon}} = \Sigma c_r \boldsymbol{\varepsilon}^{(r)} = c_0(\boldsymbol{\varepsilon}^0 + \bar{\boldsymbol{\varepsilon}}) + c_1[\boldsymbol{\varepsilon}^0 + \bar{\boldsymbol{\varepsilon}} + \langle\boldsymbol{\varepsilon}^{pt}(\theta,\phi)\rangle]$, leading to

$$\bar{\boldsymbol{\varepsilon}} = \boldsymbol{\varepsilon}^0 + c_1\langle\boldsymbol{\varepsilon}^*(\theta,\phi)\rangle. \tag{17}$$

Thus once $\langle\boldsymbol{\varepsilon}^*(\theta,\phi)\rangle$ is determined in terms of $\boldsymbol{\varepsilon}^0$, which is related to $\bar{\boldsymbol{\sigma}}$ by (8), the secant moduli tensor of the composite L_s will follow from

$$\bar{\boldsymbol{\sigma}} = L_s\bar{\boldsymbol{\varepsilon}}, \quad \text{with} \quad L_s = (3\kappa_s, 2\mu_s), \tag{18}$$

where κ_s and μ_s are the effective "secant" bulk and shear moduli of the composite at the considered $\bar{\boldsymbol{\sigma}}$.

The details for finding the average $\langle\boldsymbol{\varepsilon}^*\rangle$ in terms of $\boldsymbol{\varepsilon}^0$ have been given by Tandon and Weng (1986) for the elastic case, but the structure remains exactly identical under the elastoplastic deformation. Briefly, for each oriented inclusion the last equation of (10) is first transformed to the local axes so that connection (11) can be used. This allows one to find $\boldsymbol{\varepsilon}^*_{local}$ in terms of $\boldsymbol{\varepsilon}^0_{local}$ and $\bar{\boldsymbol{\varepsilon}}_{local}$, which in turn may be transformed back to $\boldsymbol{\varepsilon}^0$ and $\bar{\boldsymbol{\varepsilon}}$ of the material axes. We then carry out the orientational average of (16) and (17), with

$$\langle\boldsymbol{\varepsilon}^*\rangle = \frac{1}{2\pi}\int_0^\pi\int_0^\pi \boldsymbol{\varepsilon}^* \sin\theta \, d\theta \, d\phi. \tag{19}$$

This process leads to (see Tandon and Weng, 1986)

$$\bar{\varepsilon}_{kk} = (1/p_1^s - 1)\varepsilon^0_{kk}, \quad \bar{\varepsilon}'_{ij} = (1/q_1^s - 1)\varepsilon^{0\prime}_{ij}, \tag{20}$$

for the hydrostatic and deviatoric components, respectively, where

$$p_1^s = 1 + \frac{c_1}{3a}[2(S^s_{1122} + S^s_{2222} + S^s_{2233} - 1)(a_3 + a_4) + (S^s_{1111} + 2S^s_{2211} - 1)(a_1 - 2a_2)]$$

$$q_1^s = 1 - c_1\left\{\frac{2}{5}\frac{2S^s_{1212} - 1}{2S^s_{1212} + \mu_0^s/(\mu_1 - \mu_0^s)} + \frac{1}{3}\frac{2S^s_{2323} - 1}{2S^s_{2323} + \mu_0^s/(\mu_1 - \mu_0^s)}\right.$$

$$- \frac{1}{15a}[(S^s_{1122} - S^s_{2233})(2a_3 - a_4 + a_5 a) + 2(S^s_{1111} - S^s_{2211} - 1)(a_1 + a_2)$$

$$\left.(S^s_{1122} - S^s_{2222} + 1)(2a_3 - a_4 - a_5 a)]\right\}. \tag{21}$$

The constants $a_1, a_2, \ldots, a_5, a$, are given in Appendix B. In addition, one also has

$$\langle \varepsilon_{kk}^{s} \rangle = p_s \varepsilon_{kk}^{0}, \quad \langle \varepsilon_{ij}^{s'} \rangle = q_s \varepsilon_{ij}^{0'}, \tag{22}$$

where

$$p_s = p_2^s/p_1^s, \quad q_s = q_2^s/q_1^s, \tag{23}$$

and

$$\begin{aligned} p_2^s &= [a_1 - 2(a_2 - a_3 - a_4)]/3a, \\ q_2^s &= -\frac{2}{5}\frac{1}{2S_{1212}^s + \mu_0^s/(\mu_1 - \mu_0^s)} - \frac{1}{3}\frac{1}{2S_{2323}^s + \mu_0^s/(\mu_1 - \mu_0^s)} \\ &\quad + \frac{1}{15a}[2(a_1 + a_2 - a_3) + a_4 + a_5 a]. \end{aligned} \tag{24}$$

The secant bulk and shear moduli of the composite then follow from (18), (17) and (22), as

$$\frac{\kappa_s}{\kappa_0} = \frac{1}{1 + c_1 p_s}, \quad \frac{\mu_s}{\mu_0^s} = \frac{1}{1 + c_1 q_s}. \tag{25}$$

This pair of equations enables one to determine the aspect-ratio dependence of the secant moduli.

For the three particular shapes of inclusions—sphere, disc and fiber—these results take a simple form:

(i) spheres, $\alpha = 1$

$$\begin{aligned} p_1^s &= 1 + \frac{4c_1\mu_0^s(\kappa_1 - \kappa_0)}{\kappa_0(3\kappa_1 + 4\mu_0^s)}, \\ p_2^s &= -\frac{(\kappa_1 - \kappa_0)(3\kappa_0 + 4\mu_0^s)}{\kappa_0(3\kappa_1 + 4\mu_0^s)}, \\ q_1^s &= 1 + \frac{c_1(\mu_1 - \mu_0^s)(9\kappa_0 + 8\mu_0^s)}{6(\kappa_0 + 2\mu_0^s)\mu_1 + (9\kappa_0 + 8\mu_0^s)\mu_0^s}, \\ q_2^s &= -\frac{5(\mu_1 - \mu_0^s)(3\kappa_0 + 4\mu_0^s)}{6(\kappa_0 + 2\mu_0^s)\mu_1 + (9\kappa_0 + 8\mu_0^s)\mu_0^s}, \end{aligned} \tag{26}$$

$$\begin{aligned} \kappa_s &= \kappa_0^s + \frac{c_1}{\dfrac{1}{\kappa_1 - \kappa_0} + \dfrac{3c_0}{3\kappa_0 + 4\mu_0^s}}, \\ \mu_s &= \mu_0^s + \frac{c_1}{\dfrac{1}{\mu_1 - \mu_0^s} + \dfrac{6}{5}\dfrac{c_0(\kappa_0 + 2\mu_0^s)}{\mu_0^s(3\kappa_0 + 4\mu_0^s)}}. \end{aligned} \tag{27}$$

(ii) discs, $\alpha \to 0$

$$p_1^s = 1 + \frac{4c_1\mu_1(\kappa_1-\kappa_0)}{\kappa_0(3\kappa_1+4\mu_1)},$$

$$p_2^s = -\frac{(\kappa_1-\kappa_0)(3\kappa_0+4\mu_1)}{\kappa_0(3\kappa_1+4\mu_1)},$$

$$q_1^s = 1 + \frac{c_1(\mu_1-\mu_0^s)(9\kappa_1+8\mu_1)}{5\mu_0^s(3\kappa_1+4\mu_1)},$$

$$q_2^s = -\tfrac{2}{5}(\mu_1-\mu_0^s)\left[\frac{1}{\mu_1}+\frac{1}{\mu_0^s}+\frac{1}{2}\frac{3\kappa_1+4\mu_0^s}{\mu_0^s(3\kappa_1+4\mu_1)}\right], \tag{28}$$

$$\kappa_s = \kappa_1 + \frac{c_0}{-\dfrac{1}{\kappa_1-\kappa_0}+\dfrac{3c_1}{3\kappa_1+4\mu_1}},$$

$$\mu_s = \mu_1 + \frac{c_0}{-\dfrac{1}{\mu_1-\mu_0^s}+\dfrac{6}{5}\dfrac{c_1(\kappa_1+2\mu_1)}{\mu_1(3\kappa_1+4\mu_1)}}. \tag{29}$$

(iii) fibers, $\alpha \to \infty$

$$p_1^s = 1 + \frac{c_1(\kappa_1-\kappa_0)(\mu_1+3\mu_0^s)}{\kappa_0(3\kappa_1+\mu_1+3\mu_0^s)},$$

$$p_2^s = -\frac{(\kappa_1-\kappa_0)(3\kappa_0+\mu_1+3\mu_0^s)}{\kappa_0(3\kappa_1+\mu_1+3\mu_0^s)},$$

$$q_1^s = 1 + \tfrac{2}{5}c_1(\mu_1-\mu_0^s)\left[\frac{1}{\mu_1+\mu_0^s}+\frac{1}{(3-4\nu_0^s)\mu_1+\mu_0^s}+\frac{3}{2}\frac{(\kappa_1+\mu_0^s)}{\mu_0^s(3\kappa_1+\mu_1+3\mu_0^s)}\right],$$

$$q_2^s = -\tfrac{1}{5}(\mu_1-\mu_0^s)\left[\frac{4}{\mu_1+\mu_0^s}+\frac{8(1-\nu_0^s)}{(3-4\nu_0^s)\mu_1+\mu_0^s}+\frac{3\kappa_1+4\mu_0^s}{\mu_0^s(3\kappa_1+\mu_1+3\mu_0^s)}\right], \tag{30}$$

$$\kappa_s = \kappa_1 + \frac{c_0}{-\dfrac{1}{\kappa_1-\kappa_0}+\dfrac{3c_1}{3\kappa_1+\mu_1+3\mu_0^s}}$$

$$\mu_s = \mu_1 + \frac{c_0}{-\dfrac{1}{\mu_1-\mu_0^s}+\tfrac{2}{5}c_1\left[\dfrac{1}{\mu_1+\mu_0^s}+\dfrac{1}{\mu_1+\mu_0^s/(3-4\nu_0^s)}+\dfrac{1}{2}\dfrac{1}{3\kappa_1+\mu_1+3\mu_0^s}\right]}. \tag{31}$$

An interesting consequence of these results is that, although both the particle and fiber-reinforced composites are plastically compressible, a disc-reinforced composite, according to this model, remains plastically incompressible.

4. THE STRESS-STRAIN CURVE

Now let the composite be subjected to a monotonically increasing proportional loading

$$\bar{\sigma}_{ij}(t) = \alpha_{ij}\bar{\sigma}(t), \tag{32}$$

where the α_{ij} are the desired proportional constants, and $\bar{\sigma}(t)$ an increasing stress function (t being a time-like parameter). When $\bar{\sigma}(t)$ is small, the overall response is elastic, and as $\bar{\sigma}(t)$ continues to increase plastic deformation will take place.

4.1. *Elastic behavior*

In this case the overall bulk and shear moduli

$$L = (3\kappa, 2\mu) \tag{33}$$

are sufficient to describe its response. The results for this pair of moduli follow from (25), with the subscript and superscript s deleted in every term to correspond to the elastic state. For the three specific cases of spheres, discs and needles, the results are explicitly given by (27), (29) and (31), in turn. It is easily recognized that the effective moduli for the particle and disc-reinforced composites coincide with Hashin and Shtrikman's (1963) lower and upper bounds, respectively, if the inclusions are the stiffer phase. Conversely, the results are reversed when they are the softer phase. Those of the fiber- (or needle-) reinforced composite generally lie between the two (this is explicitly visible for the κ-term), and, when $\mu_1 = \mu_0$, its κ is seen to coincide with that of the disc-reinforced composite. Indeed, under this later condition all three of them lead to Hill's (1963) exact solution. The results derived for the disc case also coincide with Walpole's (1969) self-consistent estimates, and, for the needle-reinforced composite, the expressions are identical to his equation (60), provided that the properties of the effective medium—κ and μ on his right side—assume the values of the matrix κ_0 and μ_0, respectively.

4.2. *Elastoplastic behavior*

Plastic deformation commences when the yield condition of the matrix is satisfied; this occurs at $\sigma^{*(0)} = \sigma_y$. To examine this onset of yielding (in the average, not the local, sense) and the subsequent plastic deformation it is noted from (9), (20) and (8) that the effective stress of the matrix in a general elastoplastic state can be written as

$$\sigma^* = \bar{\sigma}^*/q_1^s, \tag{34}$$

where $\bar{\sigma}^*$ is the effective stress of the composite, defined as

$$\bar{\sigma}^* = (\tfrac{3}{2}\bar{\sigma}'_{ij}\bar{\sigma}'_{ij})^{1/2}. \tag{35}$$

Under the combined loading (32) it is convenient to introduce

$$\alpha^* = (\tfrac{3}{2}\alpha'_{ij}\alpha'_{ij})^{1/2}, \tag{36}$$

in parallel to (35). Then, $\bar{\sigma}^* = \alpha^*\bar{\sigma}(t)$, and the plastic deformation beings at

$$\bar{\sigma}(t) = (q_1/\alpha^*)\sigma_y, \tag{37}$$

where q_1 is the value of q_1^s, but evaluated at the elastic state (with all the sub- and superscript s deleted).

The effective stress of the matrix afterwards must satisfy its constitutive eqn (5), and this leads to

$$\bar{\sigma}(t) = (q_1^s/\alpha^*)[\sigma_y + h\cdot(\varepsilon^{p*})^n]. \tag{38}$$

Thus under an external $\bar{\sigma}_{ij}$ the average stress and strain state of the matrix can be determined iteratively in the following way. One may first assume a value for ε^{p*}, from which the values of E_0^s, ν_0^s and μ_0^s are calculated by (7), (4) and (3). These values enable one to determine the components of S_0^s, and $a_1, a_2, \ldots, a_5, a$ from the Appendix, and then q_1^s from (21) for the considered aspect ratio. With this q_1^s, the value of ε^{p*} will follow from (38) at the considered $\bar{\sigma}(t)$. If this ε^{p*} is equal, or very close to the originally assumed value, then the solution is found. Otherwise a new ε^{p*} reflecting the newly calculated value should be assumed to repeat the same process, until the true ε^{p*} is found. Once ε^{p*} is known, the values of $\sigma^{(0)}$ and $\varepsilon^{(0)}$ also follow.

For the sole purpose of generating the stress–strain curve of the composite from those of its constituents, however, such an iterative process is not necessary. In this regard one may first assume a value for ε^{p*} to begin with, from which the values of E_0^s, ν_0^s, μ_0^s, S_0^s, a_r, a and q_1^s follow in the way just described. The stress $\bar{\sigma}(t)$ then is given by (38), and so are $\bar{\sigma}_{ij}$ from (32) for the desired α_{ij}. On the other hand, the effective secant moduli $(3\kappa_s, 2\mu_s)$ are given by (25), leading to a $\bar{\varepsilon}_{ij}$ for the composite. If the plastic strains are needed, they are

$$\bar{\varepsilon}_{kk}^p = \left(\frac{1}{3\kappa_s} - \frac{1}{3\kappa}\right)\bar{\sigma}_{kk}, \quad \bar{\varepsilon}_{ij}^p = \left(\frac{1}{2\mu_s} - \frac{1}{2\mu}\right)\bar{\sigma}_{ij}'. \tag{39}$$

By increasing the value of ε^{p*} and repeating the same process, the entire stress–strain curve of the composite can be determined at a given aspect ratio and volume concentration of inclusions.

5. NUMERICAL RESULTS AND COMPARISON WITH EXPERIMENTS

It is now of interest to examine the properties of a practical system. To this end we choose the silicon-carbide/6061-aluminum composite for calculations. The elastic and plastic properties of both phases are (Arsenault, 1984; Nieh and Chellman, 1984):

silicon-carbide inclusions: $E_1 = 490$ GPa, $\nu_1 = 0.17$

aluminum matrix: $E_0 = 68.3$ GPa, $\nu_0 = 0.33$

$\sigma_y = 250$ MPa, $h = 173$ MPa and $n = 0.455$.

Using these values as the properties of the inclusions and matrix, respectively, we first examine the tensile stress–strain curves of the composite reinforced with (i) discs, (ii) fibers and (iii) spheres. The results at the three volume fractions – $c_1 = 5\%$, 10% and 20% – are depicted in Fig. 2. The shape of the inclusions is seen to have a pronounced effect on the

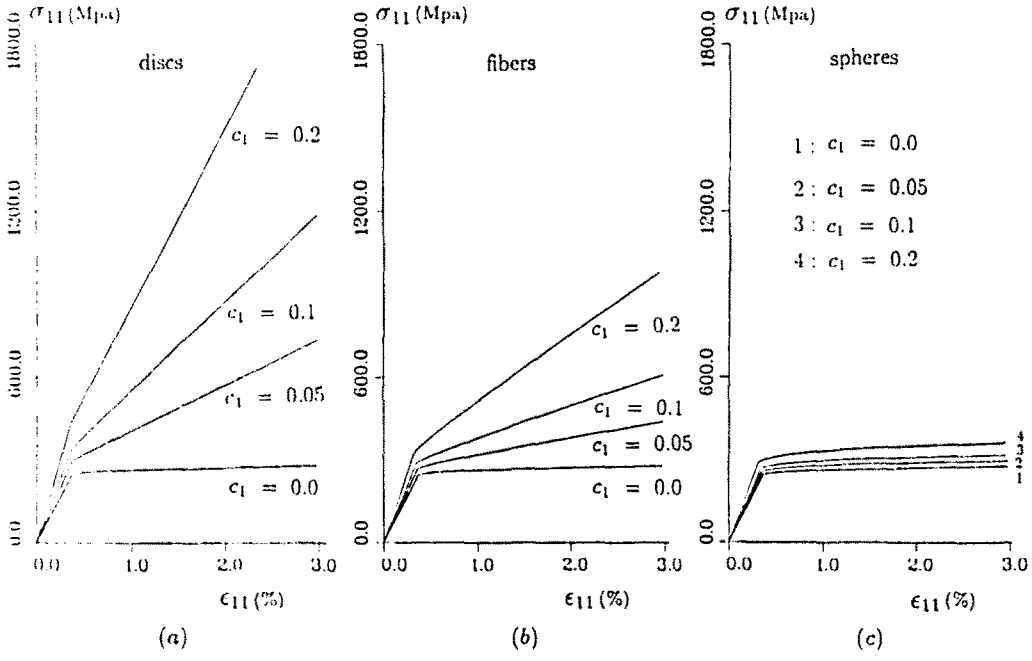

Fig. 2. Tensile stress–strain curves of silicon-carbide/aluminum composites, when the carbides exist in the form of (a) discs, (b) fibers and (c) spheres.

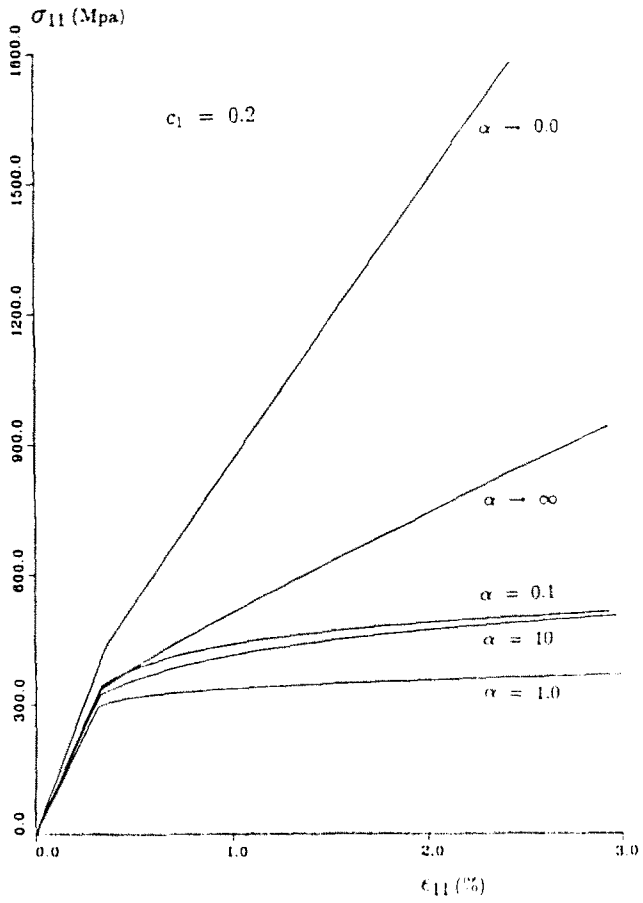

Fig. 3. The aspect-ratio dependence of the tensile stress–strain curves of the composites.

overall response. As in the elastic case, the discs provide the most effective reinforcement and the spheres are the least effective, with the fibers lying between the two.

At $c_1 = 20\%$, a more complete examination on the aspect-ratio dependence of the stress–strain curve is shown in Fig. 3 for five different aspect ratios. The work-hardening moduli are seen to improve more drastically when the aspect ratio decreases from 0.1 to 0, as compared with the corresponding increase from 10 to ∞. Within the range $0.1 < \alpha < 10$, however, the improvement appears to be about the same when the shape varies in both ways. Such a behavior is further illustrated in Fig. 4, where the stress–strain curves with $\alpha = 4$ and 1/4 are demonstrated side-by-side at three volume concentrations. In examining these three figures it also becomes evident that the overall plastic behavior of the composite is more sensitive to the inclusion shape than the elastic behavior.

The theory is finally compared with the experimental data, which were obtained by Arsenault (1984) for the same composite system with randomly oriented platelets. The average aspect ratio of the oblate inclusions is about 1/4, and $c_1 = 0.20$. The experimental results, with four different prior thickness reductions by warm rolling before the heat treatment to recover its microstructure, are depicted as discrete symbols in Fig. 5. Also shown here are the stress–strain curves of silicon carbide and 6061 aluminum. The theoretical prediction is shown as the solid line marked "Theoretical". The initial elastic response is seen to be very well predicted and, although in the plastic range the theory underestimates the flow stress somewhat, it seems to lie within a tolerable range of accuracy.

It is not clear exactly why the theory underestimates the flow stress of the composite as compared with these data. One possible reason is that carbide platelets are not exactly spheroidal and well separated in reality, but instead possess corners and may be in contact. Another possibility is attributable to the additional *in situ* hardening in the ductile aluminum matrix in the presence of the strong silicon carbides. This additional hardening is caused

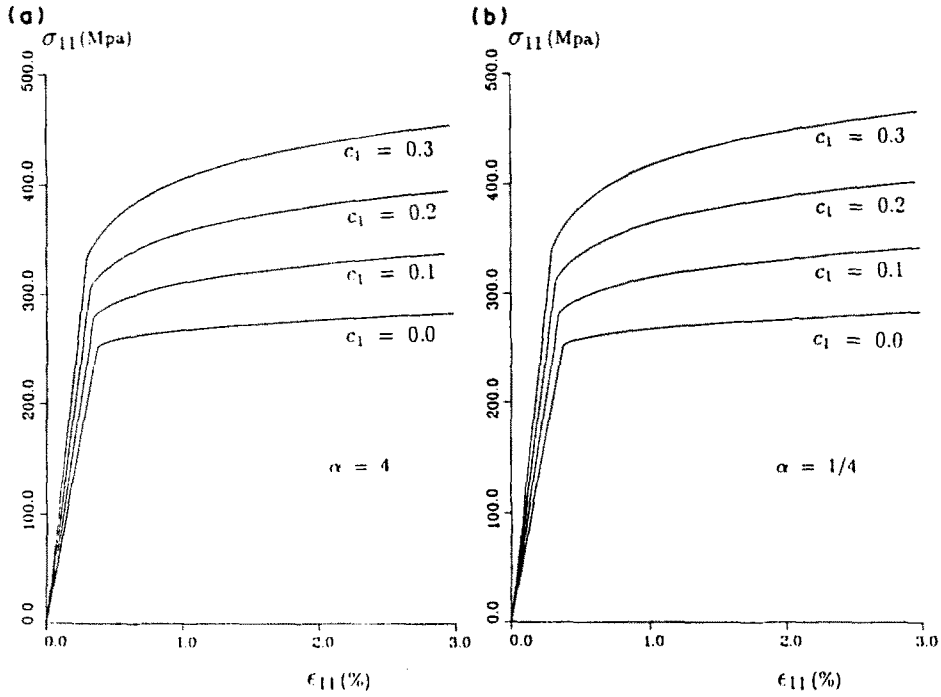

Fig. 4. The tensile stress strain relations of the composites reinforced with (a) prolate inclusions at $\alpha = 4$, and (b) oblate inclusions at $\alpha = 1/4$.

by the dislocation pile-ups against the obstacles and the long-range obstacle-dislocation interactions. At room temperature the dynamic or thermal recovery is more difficult and the pile-ups cannot climb over the obstacles as easily. Such an additional hardening is obviously not represented by the original constitutive equations of the pure matrix. In a separate study of dual-phase plasticity, Weng (1990) has also encountered similar experimental data for a dual-phase steel, where the experimental stress-strain curve even lies

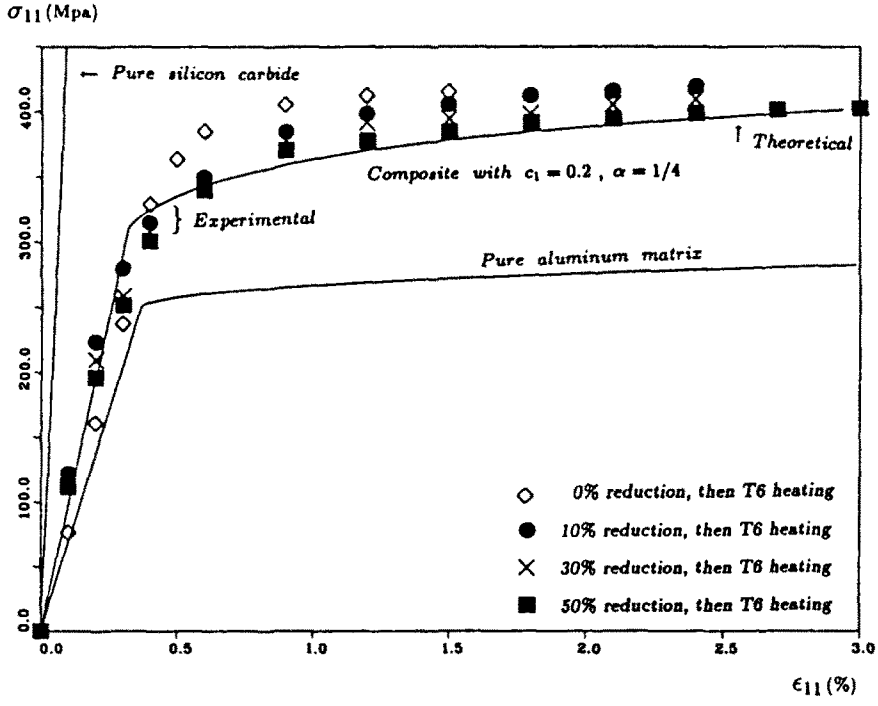

Fig. 5. Comparison between the theoretical prediction and the experimental data of a silicon-carbide/6061 aluminum composite, with platelet-type reinforcement at $\alpha = 1/4$.

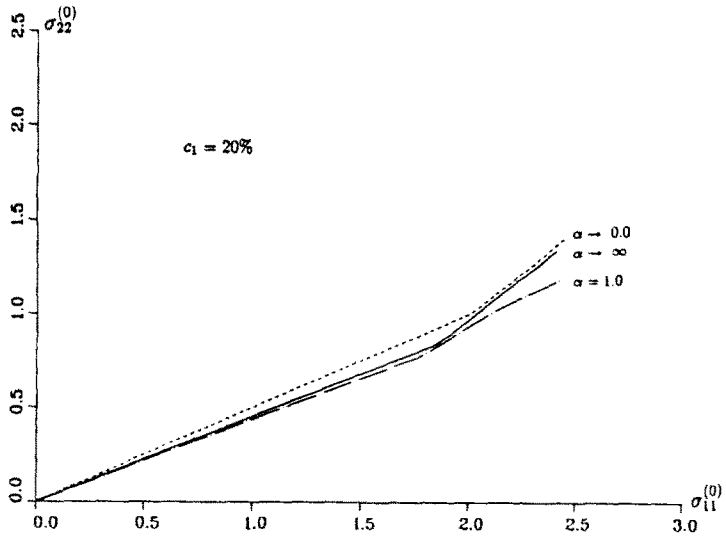

Fig. 6. Extent of deviation from strict proportionality for the average stress of the ductile matrix when the composite is under pure tension.

above the upper bound prediction of Taylor's (1938) constant total strain (without accounting for the *in situ* hardening). The precise amount of such an additional hardening, however, remains an open question and the determination of its shape and volume-fraction dependence is clearly beyond the scope of this study.

Finally we must note that, when the composite is under a proportionally increasing loading, the ductile matrix is not strictly under the proportional loading as well. The deviation from a strict proportionality, however, generally stays within Budiansky's (1959) criterion of physical soundness [which was based on Drucker's (1951) postulates in incremental plasticity]. To illustrate the aspect-ratio dependence of such a deviation, we plot in Fig. 6 the corresponding loading path of the ductile matrix in $\sigma_{11}^{(0)}$ and $\sigma_{22}^{(0)}$ space under a monotonically increasing $\bar{\sigma}_{11}$ at $c_1 = 20\%$. The initial linear portions refer to the elastic state, and the deviation commences at plastic yielding. For the considered constitutive eqn (5), the yield surface possesses no corner and, with the work-hardening exponent $n = 0.455$ for aluminum, the permissible deviation is 65° in the entire stress space. The actual deviations in Fig. 6 apparently are less than this value. Such was found to be also the case for other aspect ratios, and for other types of loading as well.

We have therefore developed a relatively simple multiaxial theory of plasticity which allows one to estimate the effect of inclusion shape on the overall stress–strain relations of a two-phase, isotropic composite. It should be recognized, however, that a mean-field approach to a nonlinear system—as mentioned in the Introduction—is usually not as accurate as a local one, but within the low-concentration range the difference between the two is not expected to be large. Thus while the mathematical structure of the theory can account for the high concentration of inclusions, in reality its application should be limited to the low concentration range.

Acknowledgement—This work was supported by the National Science Foundation, Solid and GeoMechanics Program, under Grant MSM 86-14151.

REFERENCES

Accorsi, M. L. and Nemat-Nasser, S. (1986). Bounds on the overall elastic and instantaneous elastoplastic moduli of periodic composites. *Mech. Mater.* **5**, 209–220.

Arsenault, R. J. (1984). The strengthening of aluminum alloy 6061 by fiber and platelet silicon carbide. *Mat. Sci. Engng* **64**, 171–181.

Berveiller, M. and Zaoui, A. (1979). An extension of the self-consistent scheme to plastically-flowing polycrystals. *J. Mech. Phys. Solids* **26**, 325–344.

Budiansky, B. (1959). A reassessment of deformation theories of plasticity. *J. Appl. Mech.* **26**, 259–264.

Christensen, R. M. (1979). *Mechanics of Composite Materials*. John Wiley, New York.
Chu, T. Y. and Hashin Z. (1971). Plastic behavior of composites and porous media under isotropic stress. *Int. J. Engng Sci.* **9**, 971–994.
Drucker, D. C. (1951). A more fundamental approach to plastic stress–strain relations. *Proc. 1st U.S. Natl. Congr. Appl. Mech.*, pp. 487–491. ASME, New York.
Eshelby, J. D. (1957). The determination of the elastic field of an ellipsoidal inclusion, and related problems. *Proc. R. Soc. London* **A241**, 376–396.
Hashin, Z. and Shtrikman, S. (1963). A variational approach to the theory of the elastic behavior of multiphase materials. *J. Mech. Phys. Solids* **11**, 127–140.
Hill, R. (1963). Elastic properties of reinforced solids: Some theoretical principles. *J. Mech. Phys. Solids* **11**, 357–372.
Hill, R. (1964). Theory of mechanical properties of fiber-strengthened materials: II. Inelastic behavior. *J. Mech. Phys. Solids* **12**, 213–218.
Hill, R. (1965). Continuum micro-mechanics of elastoplastic polycrystals. *J. Mech. Phys. Solids* **13**, 89–101.
Mori, T. and Tanaka, K. (1973). Average stress in the matrix and average elastic energy of materials with misfitting inclusions. *Acta Metall.* **21**, 571–574.
Mura, T. (1987). *Micromechanics of Defects in Solids*, 2nd Edn. Martinus Nijhoff, Dordrecht.
Nieh, T. G. and Chellman, D. J. (1984). Modulus measurements in discontinuous reinforced aluminum composites. *Scripta Metall.* **18**, 925–928.
Talbot, D. R. S. and Willis, J. R. (1987). Bounds and self-consistent estimates for the overall properties of nonlinear composites. *IMA J. Appl. Math.* **39**, 215–240.
Tandon, G. P. and Weng, G. J. (1986). Average stress in the matrix and effective moduli of randomly oriented composites. *Composite Sci. Tech.* **27**, 111–132.
Tandon, G. P. and Weng, G. J. (1988). A theory of particle-reinforced plasticity. *J. Appl. Mech.* **55**, 126–135.
Taylor, G. I. (1938). Plastic strain in metals. *J. Inst. Metals* **62**, 307–324.
Teply, J. L. and Dvorak, G. J. (1988). Bounds on overall instantaneous properties of elastic–plastic composites. *J. Mech. Phys. Solids* **36**, 29–58.
Walpole, L. J. (1969). On the overall elastic moduli of composite materials. *J. Mech. Phys. Solids* **17**, 235–251.
Weng, G. J. (1982). A unified, self-consistent theory for the plastic-creep deformation of metals. *J. Appl. Mech.* **49**, 728–734.
Weng, G. J. (1984). Some elastic properties of reinforced solids, with special reference to isotropic ones containing spherical inclusions. *Int. J. Engng Sci.* **22**, 845–856.
Weng, G. J. (1990). The overall elastoplastic stress–strain relations of dual-phase metals. *J. Mech. Phys. Solids* **38**, 419–441.
Wu, T. T. (1966). The effect of inclusion shape on the elastic moduli of a two-phase material. *Int. J. Solids Structures* **2**, 1–8.

APPENDIX A: ESHELBY'S S-TENSOR IN TERMS OF THE SECANT MODULI

For a spheroidal inclusion with the symmetric axis identified as x_1, the components of Eshelby's tensor S^s_{ijkl} are

$$S^s_{1111} = \frac{1}{2(1-\nu_0^s)}\left\{1-2\nu_0^s+\frac{3\alpha^2-1}{\alpha^2-1}-\left[1-2\nu_0^s+\frac{3\alpha^2}{\alpha^2-1}\right]g\right\},$$

$$S^s_{2222} = S^s_{1111} = \frac{3}{8(1-\nu_0^s)}\frac{\alpha^2}{\alpha^2-1}+\frac{1}{4(1-\nu_0^s)}\left[1-2\nu_0^s-\frac{9}{4(\alpha^2-1)}\right]g,$$

$$S^s_{2211} = S^s_{1122} = \frac{1}{4(1-\nu_0^s)}\left\{\frac{\alpha^2}{2(\alpha^2-1)}-\left[1-2\nu_0^s+\frac{3}{4(\alpha^2-1)}\right]g\right\},$$

$$S^s_{2211} = S^s_{1111} = -\frac{1}{2(1-\nu_0^s)}\frac{\alpha^2}{\alpha^2-1}+\frac{1}{4(1-\nu_0^s)}\left\{\frac{3\alpha^2}{\alpha^2-1}-(1-2\nu_0^s)\right\}g,$$

$$S^s_{1122} = S^s_{1111} = -\frac{1}{2(1-\nu_0^s)}\left[1-2\nu_0^s+\frac{1}{\alpha^2-1}\right]+\frac{1}{2(1-\nu_0^s)}\left[1-2\nu_0^s+\frac{3}{2(\alpha^2-1)}\right]g,$$

$$S^s_{2323} = \frac{1}{4(1-\nu_0^s)}\left\{\frac{\alpha^2}{2(\alpha^2-1)}+\left[1-2\nu_0^s-\frac{3}{4(\alpha^2-1)}\right]g\right\},$$

$$S^s_{1212} = S^s_{1313} = \frac{1}{4(1-\nu_0^s)}\left\{1-2\nu_0^s-\frac{\alpha^2+1}{\alpha^2-1}-\frac{1}{2}\left[1-2\nu_0^s-\frac{3(\alpha^2+1)}{\alpha^2-1}\right]g\right\}. \tag{A1}$$

where ν_0^s is the secant Poisson's ratio of the matrix (or more precisely the Poisson ratio of the linearly elastic comparison material), α is the aspect ratio of the inclusion ($=l/d$), and g is given by

$$q = \frac{\alpha}{(\alpha^2-1)^{3/2}}\{\alpha(\alpha^2-1)^{1/2} - \cosh^{-1}\alpha\}, \quad \text{prolate shape.} \tag{A2}$$

$$= \frac{\alpha}{(1-\alpha^2)^{3/2}}\{\cos^{-1}\alpha - \alpha(1-\alpha^2)^{1/2}\}, \quad \text{oblate shape.} \tag{A3}$$

For a spherical inclusion, they simplify to

$$S^*_{1111} = S^*_{2222} = S^*_{3333} = \frac{7-5\nu_0^*}{15(1-\nu_0^*)},$$

$$S^*_{1122} = S^*_{2233} = S^*_{3311} = \frac{5\nu_0^*-1}{15(1-\nu_0^*)},$$

$$S^*_{1212} = S^*_{2323} = S^*_{3131} = \frac{4-5\nu_0^*}{15(1-\nu_0^*)}. \tag{A4}$$

For a needle or circular cylinder with $\alpha \to \infty$, we have

$$S^*_{1111} = 0,$$

$$S^*_{2222} = S^*_{3333} = \frac{5-4\nu_0^*}{8(1-\nu_0^*)},$$

$$S^*_{2211} = S^*_{3322} = \frac{4\nu_0^*-1}{8(1-\nu_0^*)},$$

$$S^*_{2233} = S^*_{3311} = \frac{\nu_0^*}{2(1-\nu_0^*)}$$

$$S^*_{1122} = S^*_{1133} = 0,$$

$$S^*_{2323} = \frac{3-4\nu_0^*}{8(1-\nu_0^*)},$$

$$S^*_{1212} = S^*_{1313} = \frac{1}{4}. \tag{A5}$$

For a thin disc with $\alpha \to 0$, the only nonvanishing components are

$$S^*_{1111} = 1,$$

$$S^*_{1122} = S^*_{1133} = \frac{\nu_0^*}{1-\nu_0^*},$$

$$S^*_{1212} = S^*_{1313} = \frac{1}{2} \tag{A6}$$

APPENDIX B: COMPONENTS OF $a_1, \ldots, a_5, a$

$$a_1 = 6(\kappa_1-\kappa_0)(\mu_1-\mu_0^*)(S^*_{2222}+S^*_{2211}-1) - 2(\kappa_0\mu_1-\kappa_1\mu_0^*) + 6\kappa_1(\mu_1-\mu_0^*),$$

$$a_2 = 6(\kappa_1-\kappa_0)(\mu_1-\mu_0^*)S^*_{1133} + 2(\kappa_0\mu_1-\kappa_1\mu_0^*),$$

$$a_3 = -6(\kappa_1-\kappa_0)(\mu_1-\mu_0^*)S^*_{3311} - 2(\kappa_0\mu_1-\kappa_1\mu_0^*),$$

$$a_4 = 6(\kappa_1-\kappa_0)(\mu_1-\mu_0^*)(S^*_{1111}-1) + 2(\kappa_0\mu_1-\kappa_1\mu_0^*) + 6\mu_1(\kappa_1-\kappa_0),$$

$$a_5 = 1.[S^*_{1122}-S^*_{1111}+1-\mu_1/(\mu_1-\mu_0^*)].$$

$$a = 6(\kappa_1-\kappa_0)(\mu_1-\mu_0^*)[2S^*_{1133}S^*_{3311} - (S^*_{1111}-1)(S^*_{1122}+S^*_{1133}-1)] + 2(\kappa_0\mu_1-\kappa_1\mu_0^*)[2(S^*_{1133}+S^*_{3311}) + (S^*_{1111}-S^*_{1122}-S^*_{3311})] - 6\kappa_1(\mu_1-\mu_0^*)(S^*_{1111}-1) - 6\mu_1(\kappa_1-\kappa_0)(S^*_{2222}+S^*_{2211}-1) - 6\kappa_1\mu_1.$$